Ultraviolet Luminescence from Defect Complexes in the Twin Boundaries of K-Feldspar

Luis Sánchez-Muñoz,*,† Javier García-Guinea,‡ Jesús Sanz,§ Virgilio Correcher,† and Antonio Delgado†

CIEMAT, Avda Complutense 22, Madrid 28040, Spain, Museo Nacional de Ciencias Naturales (MNCN-CSIC), C/ Jose Gutierrez Abascal 2, Madrid 28006, Spain, and Instituto de Ciencia de Materiales de Madrid (ICMM-CSIC), Cantoblanco, Madrid 28049, Spain

Received February 1, 2006. Revised Manuscript Received May 12, 2006

The ultraviolet (UV) emission at 290 nm has been studied by thermoluminescence (TL), cathodoluminescence (CL), and radioluminescence (RL) techniques in a natural K-feldspar with intermediate microcline X-ray diffraction pattern. Electron microprobe analyses (EMPA) give the chemical formula $K_{0.98}Na_{0.02}Al_{1.02}Si_{2.98}O_8$. An irregular submicroscopical twinning has been observed from transmission electron microscopy (TEM) images. Selected area electron diffraction (SAED) patterns along the [001] zone axis evidence the triclinic character of this feldspar (γ^* angle $\approx 91°$) and exhibit a double spot splitting, associated with the presence of discrete twin-domains, interconnected by diffuse streaks. The ^{29}Si MAS NMR spectrum demonstrates that the appearance of this UV emission cannot be explained by distinct T−O−T geometry of the local structure in comparison with other triclinic K-feldspars. The close association between twinning and the UV band in the K-feldspar points to charge trapping and light emissions from complexes of structural defects located at the twin-domain boundaries. The high-temperature slope of the TL glow curve follows a power law decay, suggesting possible trapping−detrapping dynamics related to cooperative phenomena inside the complexes.

Introduction

The luminescence properties of natural feldspars are usually employed for geological or archaeological dating purposes of sediments and ceramic artifacts,[1] identification of irradiated food, environmental retrospective dosimetry,[2] remote "in situ" mineral identification,[3] and space dosimetry.[4] In addition, the aluminosilicate framework of feldspars, with an appropriate tuning of the activator content, is being used in synthetic phosphors for ultraviolet light-emitting diodes,[5] long-lasting phosphoresce materials,[6] and plasma display panels.[7] The luminescence characteristics of feldspars, spanning the whole of the visible spectrum including the ultraviolet (UV) spectral region, are strongly related to the mineral type. Early experiments of Marfunin demonstrated that the brightness increases with the triclinic character of feldspars.[8] It indicates that the sensitivity to ionizing radiations and the efficient recombination processes are directly related to some defects produced during the monoclinic−triclinic transition.

The structure of alkali feldspars consists of a three-dimensional framework of corner-sharing AlO_4 and SiO_4 tetrahedra (T sites) in which K and Na ions occupy large structural cavities (M sites). At higher temperatures, Na- and K-feldspars exhibit a continuous solid solution series; however, during cooling, exolution processes produce K- and Na-rich phases with perthitic textures. The stable high-T phase in K-feldspars is sanidine (monoclinic, *C*2/*m*) with a local Si/Al disorder in two tetrahedral sites, T_1 and T_2. On cooling, a monoclinic−triclinic phase transition (MTT) can occur in which coexist not only a Si/Al order−disorder component, but also a cooperative displacive component. As a result of the phase transition, a domain structure is developed in microcline or the low-T phase (triclinic, $C\bar{1}$) with four nonequivalent sites, T_{1o}, T_{1m}, T_{2o}, and T_{2m}.[9] Several varieties of microcline have been defined as follows: (i) high microclines (or orthoclase) showing a modulated structure with "tweed" contrast TEM images;[10,11] (ii) intermediate microclines displaying an irregular twinning with Albite (reflection in [010]) and Pericline (two-fold rotation about [010]) twin laws at the submicroscopical scale;[12] and (iii) low microclines composed by a regular and coarse twin-

* Corresponding author. Tel.: +34-91-346-6322. Fax: +34-91-346-6714. E-mail: luis.sanchez@ciemat.es.
† CIEMAT.
‡ MNCN-CSIC.
§ ICMM-CSIC.

(1) Hutt, G.; Jaek, I.; Tchonka, J. *Q. Sci. Rev.* **1988**, *7*, 381−385.
(2) Correcher, V.; Gómez-Ros, J. M.; Delgado, A. *Radiat. Prot. Dosim.* **1999**, *84*, 547−549.
(3) Takaki, S.; Ikeya, M.; Yamanaka, C. *Radiat. Meas.* **1997**, *27*, 393−397.
(4) Benoit, P. H.; Chen, Y. *Radiat. Meas.* **1996**, *26*, 281−289.
(5) Yang, W. J.; Luo, L. Y.; Chen, T. M.; Wang, N. S. *Chem. Mater.* **2005**, *17*, 3883−3888.
(6) Wang, Y. H.; Wang, Z. Y.; Zhang, P. Y.; Hong, Z. L.; Fan, X. P.; Quan, G. D. *Mater. Lett.* **2004**, *58*, 3308−3311.
(7) Im, W. B.; Kim, Y.-I.; Kang, J. H.; Jeon, D. Y. *Solid State Commun.* **2005**, *134*, 717−720.
(8) Marfunin, A. S. *Spectroscopy, Luminescence and Radiation Centres in Minerals*; Springer-Verlag: Berlin, 1979.
(9) Smith, J. V.; Brown, W. L. *Feldspar Minerals*, 2nd ed.; Springer-Verlag: Berlin, 1988.
(10) McConnell, J. D. C. *Philos. Mag.* **1965**, *11*, 1289−1301.
(11) Sánchez-Muñoz, L. L.; Nistor, G.; Van Tendeloo, J.; Sanz, J. *J. Electron Microsc.* **1998**, *47*, 17−28.
(12) Bambauer, H. U.; Krause, C.; Kroll, H. *Eur. J. Mineral.* **1989**, *1*, 47−58.

10.1021/cm060246o CCC: $33.50
Published on Web 06/09/2006

Table 1. Chemical Composition of Sample LS176 from Electron Microprobe Analyses[a]

SiO_2	63.63	63.04	64.38	62.59	63.57	62.80	63.04	63.36
Al_2O_3	18.65	18.49	18.89	19.14	18.55	18.70	18.75	18.46
FeO			0.03	0.09	0.32	0.04	0.07	0.05
MnO	0.01			0.01	0.02			
MgO	0.01	0.02			0.03	0.01		0.02
CaO	0.02	0.03	0.01	0.02	0.05			0.02
Na_2O	0.29	0.37	0.23	0.26	0.29	0.23	0.26	0.27
K_2O	16.52	16.49	16.72	16.65	16.91	16.60	16.61	16.95
TiO_2						0.01	0.01	
NiO		0.04		0.06	0.05	0.04	0.06	
Cr_2O_3				0.03				
P_2O_5			0.01	0.01		0.03	0.05	
F		0.01						
Cl	0.03	0.06	0.01	0.04	0.05	0.01	0.02	0.01
total	99.16	98.20	100.28	98.90	99.82	98.48	98.87	99.15

[a] Analyses are given in weight percentages of oxides.

domain structure.[13] As triclinicity increases from high-to-low microclines (γ^* angle from ~90° to 92.5°), Al ions are progressively ordered into T_{1o} sites.

Feldspar luminescence shows three contrasting types of light emissions, as follows: (i) Transition metal ions are incorporated as impurities, for example, Mn^{2+} as extrinsic point defects emitting ca. 570 nm,[14] producing isometric emission bands. (ii) Electron−hole recombinations at lattice defects represent the "broad blue band" case, that is, between 400 and 500 nm. On the basis of EPR results, this band has been ascribed to holes trapped on oxygen atoms bounded to Al ions ($Al-O^--Al$ centers).[8,15] (iii) Intrinsic defects of feldspars, for example, the UV emission bands, are related to irreversible changes in the luminescence characteristics with temperature.[16] The UV bands exhibiting orientation dependence indicate a relationship with structural elements.[17]

In particular, the intensity of the 290 nm band is mainly correlated with the structural state of K-rich feldspars.[18,19] Nevertheless, several interpretations have been given to such 290 nm band, as follows: (i) from a point defect approach, Pb^{2+} at an unidentified lattice site and Tl^+ substituting for K^+ site;[20] (ii) from a cluster defect viewpoint, a $Pb-O^--\bullet\bullet X$ hole center with a small divalent impurity ion X of as yet unidentified nature and incorporation of Pb impurities into K^+ sites;[15] and (iii) from an intrinsic defects perspective, a relationship with the ionic motion of metastable accumulated Na atoms along interface-interphases of the material has been proposed.[16] This interpretation was supported by the observed behavior of high microcline in which its light emission changes sharply in intensity and slightly in position with mechanical treatments and preheating at low temperatures, showing an unstable character.[21]

These hypotheses have been proposed from experimental works using perthitic feldspar samples with exsolved Na and K phases (see review in ref 22). Furthermore, the 290 nm band is frequently observed also in pure Na-feldspar crystals, but it has not been detected in unexsolved K-feldspars. Therefore, the origin of the 290 nm luminescence emission in feldspars is an important feature requiring extra research. The aim of this work is to investigate the origin of this UV luminescence band by TL, RL, and CL techniques on a homogeneous triclinic K-feldspar. The additional characterization of this homogeneous sample by XRD, NMR, and TEM techniques allows us to correlate the origin of the UV luminescence with explicit structural features.

Experimental Section

Material. Measurements were performed on a natural reddish opaque adularia sample (specimen LS176) collected from a hydrothermal fracture filling in El Verdugal granitic pegmatite from Colmenar Viejo (Madrid, Spain).[23] This adularia sample is an intergrowth of several small crystal sized 1 cm and is iron-oxide stained. Separated Na-feldspar phases and Albite−Pericline twinning cannot be detected by optical microscopy.

Electron Microprobe. Nondestructive chemical analyses of major and minor elements were performed by electron microprobe analysis (EMPA) to provide information on the chemical homogeneity of the adularia crystal (Table 1). The sample was bound together with a polymer and softly polished, offering a flat surface to the EMPA beam. The crystal-chemical characteristics of the feldspar were determined on data series of electron microprobe analyses (JEOL Superprobe JXA-8900M), bulk and channel-selected (TAP, PETJ, LIF, PETH) X-ray spectra search, and by identification routines. The used standards were natural and synthetic crystals from the collection of the "Servicio de Microscopía Electrónica Lluis Bru", Universidad Complutense de Madrid. The ZAF program was used for correction of matrix effects. Natural K-rich feldspars, Na-feldspar, and pure synthetic K-feldspar standards were previously analyzed by the electron probe in several experimental conditions to obtain maximum signal and minimum Na loss. The spot diameter of the probe was ca. 5 μm, and the operating conditions were 15 kV and 20 nA.

X-ray Fluorescence. Bulk analyses of major, minor, and trace elements (Table 2) were carried out by spectrometry of X-ray fluorescence (XRF) using a PHILIPS PW-1404 with an Sc−Mo tube, using Ge, LIF220, LIF200, PE, and TLAP as analyzer crystals

(13) Fitz Gerald, J. D.; McLaren, A. C. *Contrib. Mineral. Petrol.* **1982**, *80*, 219−229.
(14) Geake, J. E.; Walker, G.; Telfer, D. J.; Mills, A. A.; Garlick, G. F. J. *Geochim. Cosmochim. Acta* **1973**, *4*, 3181−3189.
(15) Speit, B.; Lehmann, G. *Phys. Chem. Miner.* **1982**, *8*, 77−82.
(16) García-Guinea, J.; Townsend, P. D.; Sánchez-Muñoz, L.; Rojo, J. M. *Phys. Chem. Miner*. **1999**, *26*, 658−667.
(17) Finch, A. A.; Hole, D. E.; Townsend, P. D. *Phys. Chem. Miner*. **2003**, *30*, 373−381.
(18) García-Guinea, J.; Rendell, H. M.; Sánchez-Muñoz, L. *Radiat. Prot. Dosim*. **1996**, *66*, 395−398.
(19) Clarke, M. L.; Rendell, H. M.; Sánchez-Muñoz, L.; García-Guinea, J. *Radiat. Meas*. **1997**, *27*, 137−144.
(20) Prescott, J. R.; Fox, P. J. *J. Phys. D: Appl. Phys.* **1993**, *26*, 2245−2254.
(21) Garcia-Guinea, J.; Correcher, V. *Spectrosc. Lett.* **2000**, *33*, 103−113.
(22) Krbetschek, M. R.; Götze, J.; Dietrich, A.; Trautman, T. *Radiat. Meas.* **1997**, *27*, 695−748.
(23) Sanchez-Munoz, L. Relationship between Na/K exsolution and the structural-microtextural characteristics of pegmatitic alkali feldspars. Ph.D. Thesis, Universidad Complutense de Madrid, Spain, 1992.

Table 2. Chemical Composition of Sample LS176 from X-ray Fluorescence[a]

oxide	%	traces	ppm
SiO_2	63.12	Sr	17
Al_2O_3	18.74	Zr	16
Fe_2O_3	0.29	Y	23
MnO	0.03	Ni	10
MgO	0.02	Co	4
CaO	0.58	Cr	12
Na_2O	0.19	Th	8
K_2O	16.59	Nb	186
TiO_2	0.01	La	3
P_2O_5	0.48	Zn	5
Rb	782	Cs	15
Ba	76	Pb	6

[a] Analyses are given in weight percentages for major and minor elements and ppm for trace elements. L.I. = 0.51 wt %.

and Super-Q manager from Panalytical-Spain as analytical software, in Museo Nacional de Ciencias Naturales (CSIC) using pellets of 8 g of milled sample with 0.1 g of elbacite pressed under 20 TM and dried at 40 °C in a climatic chamber.

X-ray Diffraction. The specimen was studied by powder X-ray diffraction (XRD) using a Siemens D-5000 automated diffractometer with Cu Kα radiation at 40 kV and 30 nA with Si as internal standard. Patterns were obtained by step scanning from 2° to 64° 2θ in steps of 0.020°, and a counting time of 6 s per step.

NMR. High-resolution ^{29}Si MAS NMR spectroscopy of powdered samples was recorded at 79.49 MHz, by spinning the sample at the magic angle (54°44′) in a Bruker MSL-400 spectrometer equipped with a Fourier transform unit, in ICMM (Madrid, Spain). A spinning frequency of the sample sited in the range 4000−5000 cps. $\pi/2$ (4 μs) pulses have been used to record Si signal ($I = {}^1/_2$). The delay for the ^{29}Si signal recycle time value was 1800 s to avoid saturation effects. Chemical shifts are reported in parts per million (ppm) from external tetramethylsilane (TMS) at room temperature for the Si spectrum, and the mean error in the measured chemical shift of each component was 0.2 ppm. The chemical shift or shielding is the most practical parameter obtained in NMR experiments, as it indicates the degree to which nearby electrons shield the Si nucleus from the external magnetic field. Si atoms in different crystallochemical sites are shielded differently and thus absorb energy at different frequencies. The measured differences are within thousandths of a part per million. Fifty free induction decays (FIDs) were utilized for the Si signal. The ^{29}Si NMR spectrum has been fitted by using the Bruker WINFIT program. Several Gaussian components with different line widths were used to reproduce the Si spectrum as developed in ref 11.

Electron Microscopy. Transmission electron microscopy (TEM) micrographs and selected area electron diffraction (SAED) patterns along the [001] zone axis (a^*b^* plane) were obtained with a Tecnai 20T (PHILIPS) apparatus working at 200 kV (Universidad Juan Carlos I, Madrid, Spain). The sample used in this analysis was obtained by crushing a fragment of the original sample; it exhibits a pronounced (001) cleavage plane. Special care was taken to minimize the electron irradiation damage.

Luminescence Spectroscopies. Spectra were performed on cleaved chips of 3 × 3 × 2 mm^3 (~5 mg) of LS176 sample mounted with silicone oil onto an aluminum disk using the 3D thermoluminescence (TL) spectrometer of Sussex University. Signals were recorded over the 200−800 nm wavelength range, with a resolution of 5 nm for 100 point spectra, and 3 nm for 200 point spectra. All signals were corrected for the spectral response of the system. The radioluminescence (RL) was obtained during excitation, and then samples were heated to 400 °C at 2.5 °C s^{-1} while the TL spectra were recorded. Prior to TL measurements (recorded in the range of 20−400 °C), samples were 50 Gy X-irradiated and stored for 24 h under red light. Cathodoluminescence (CL) experiments were performed using an electron beam with a current of 0.4 μA and a voltage of 10 kV at room temperature. The X-ray unit tube was a Phillips MG MCN 101 X-ray tube with a current of 5 mA and a voltage of 5 kV delivering a dose rate of 10 Gy min^{-1} to the sample. Sample processing and measurements were made under red light to avoid the release of the trapped electrons from the semistable sites into hole centers (including luminescence centers) due to light sensitivity.

Results

Chemical Composition. Tables 1 and 2 show the sample has a very low Na content, in comparison with most of the igneous and metamorphic perthitic microclines and some hydrothermal adularias with orthoclase X-ray pattern. This sodium shortage is also observed in adularias collected from open fractures in granitic pegmatites. The iron oxide content is related to the reddish color of the sample. The Cl content values agree with the hydrothermal origin, the Pb content is very low in comparison with some amazonite feldspars, and the Mn amount is at the detection limit in EMPA but clearly detected by XRF. The Tl content is lower that the detection limit of these techniques. Because Ca was always at very low concentration, an Or_xAb_y molar expression ($x + y = 100$) is used to show the proportions of K-feldspar and Na-feldspar in the solid solution; that is, the average composition of the sample is $Or_{98}Ab_2$ ($K_{0.98}Na_{0.02}Al_{1.02}Si_{2.98}O_8$).

X-ray Diffraction. The XRD pattern of the K-feldspar showed that the analyzed crystal is composed mainly by only one microcline variety and also that Na-feldspar from exolution domains and quartz impurities cannot be detected. Three structural parameters were estimated from the XRD patterns, as follows:

(i) Triclinicity, Δ, is a parameter defined by the splitting of the $(131)-(1\bar{3}1)$ peaks, and, linked with the structural distortion from the monoclinic symmetry, it varies from 0.0 in high microcline to 1.0 in low microcline. In the sample, the Δ value was 0.78.

(ii) Parameter $\sum t_1 = t_{1o} + t_{1m}$ reports on the Si/Al order because it defines the content of Al ions in T_{1o} and T_{1m} positions; it is calculated from the (060) and $(\bar{2}04)$ peaks.[24] The X-ray pattern gives a value of $\sum t_1 = t_{1o} + t_{1m} = 0.952$.

(iii) Parameter $\Delta t_1 = t_{1o} - t_{1m}$ also reports on the Si/Al order because it states the difference from Al ions in the T_{1o} and T_{1m} positions being calculated from the second moment of the X-ray profile in the region of the $(131)-(1\bar{3}1)$ splitting.[23] The calculated value of $\Delta t_1 = t_{1o} - t_{1m}$ was 0.766.

From these values, the K-feldspar variety corresponds to an intermediate microcline. When derived from the high-T phase by the MTT, microcline shows a twin-domain structure with inversion domain boundaries. This material cannot be synthesized in the laboratory as it is related to the very sluggish Si/Al ordering in the tetrahedral sites. Consequently, luminescence studies of these microclines can only be done with natural samples.

(24) Kroll, H.; Ribbe, P. H. *Am. Mineral.* **1987**, *72*, 491−506.

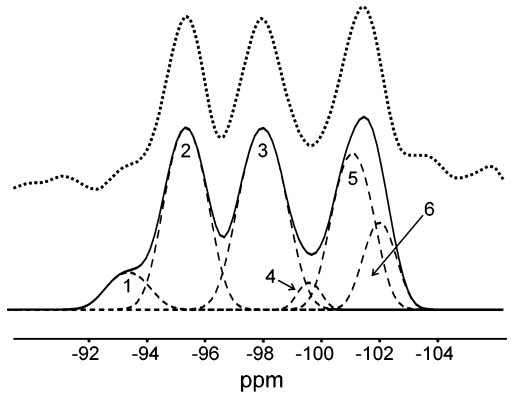

Figure 1. Experimental (dotted line) and calculated (solid line) ^{29}Si MAS NMR spectra of the intermediate microcline LS176 showing the next six components corresponding to Si in the following crystallochemical sites (dashed lines): 1, T_{20} (2Si,2Al) at −93.1 ppm; 2, T_{2m} (2Si,2Al) at −95.1 ppm; 3, T_{20} (3Si,1Al) at −97.7 ppm; 4, T_{2m} (3Si,1Al) at −99.4 ppm; 5, T_{1m} (3Si,1Al) at −100.9 ppm; and 6, T_{10} (3Si,1Al) at −101.9 ppm.

NMR Spectroscopy. Local order in the Si/Al distribution of the tetrahedral framework of the LS176 adularia has been studied by ^{29}Si MAS NMR spectroscopy. Figure 1 shows the experimental ^{29}Si spectrum that is composed of three maxima at −95.1, −97.6, and −101.0 ppm located at the typical positions of the triclinic $C\bar{1}$ K-feldspars. Four crystallographic nonequivalent tetrahedral positions are distinguished in triclinic K-feldspars: T_{10}, T_{1m}, T_{20}, and T_{2m}. The T_{10} site is surrounded by $1T_{1m}$, $1T_{20}$, and $2T_{2m}$ tetrahedra; the T_{1m} by $1T_{10}$, $1T_{2m}$, and $2T_{20}$; the T_{20} by $1T_{10}$, $1T_{2m}$, and $2T_{1m}$; and the T_{2m} by $1T_{1m}$, $1T_{20}$, and $2T_{10}$. The configuration of maximum local order, low microcline end member with maximum triclinicity, occurs when all Al atoms are located in the T_{10} site and Si atoms are occupying the other three sites. In this case, the ^{29}Si spectrum is formed by three bands with equal intensity, −100.8 ppm corresponding to T_{1m} (3Si,1Al), −97.9 ppm to T_{20} (3Si,1Al), and −95.0 to T_{2m} (2Si,2Al).

When some Si atoms are in T_{10} sites, new chemical environments are detected in the ^{29}Si spectrum. Specifically two new bands separated by ∼4.5 ppm are detected when Al atoms are incorporated to T_{1m}, T_{20}, and T_{2m} sites: the band at −93.1 ppm corresponds to Si atoms in T_{20} surrounded by 2Si,2Al, and the band at −99.4 ppm corresponds to Si in T_{2m} surrounded by 3Si,1Al. An additional band at −101.9 ppm, associated with Si in T_{10} (3Si,1Al) environments, was also included in this analysis. Figure 1 shows the fitting of the ^{29}Si NMR spectrum with six Gaussian components of 1.5 ppm of line width. All deduced parameters (position, line width, integrated intensity of peaks) were refined to a 95% confidence limit (see Table 3 for details). As shown in Figure 1, the dashed lines correspond to the calculated fitted peaks, which make up the calculated profile (solid line). From the quantitative analysis of NMR spectrum, occupancies of tetrahedral sites t_{10}, t_{1m}, t_{20}, and t_{2m} by Al were calculated: 0.821, 0.158, 0.017, and 0.002. Finally, $\sum t_1 = t_{10} + t_{1m} = 0.979$ and $\Delta t_1 = t_{10} - t_{1m} = 0.663$ values acquired from NMR agree reasonably well with those obtained from XRD data ($\sum t_1 = 0.952$ and $\Delta t_1 = 0.766$).

TEM Image and SAED Pattern. The presence of twinning-tweed structures in microclines was investigated by TEM, analyzing the [001] zone axis or a^*b^* plane. Figure 2 is a conventional bright-field low-resolution image along this zone axis showing a heterogeneous and irregular microstructure due to an orthogonal structure with a wavelike contrast. In this figure, some small ill-defined regions with homogeneous contrast correspond to domains after the Albite and Pericline twin laws. The difference in contrast between domains is not sharp but gradual. These microstructural characteristics coincide with those of irregular microcline.

Table 3. Parameters from ^{29}Si MAS NMR of LS176[a]

position (ppm)	integrated intensities	structural sites
−93.1	2.48	T_{20} (2Si,2Al)
−95.1	29.50	T_{2m} (2Si,2Al)
−97.7	30.27	T_{20} (3Si,1Al)
−99.4	3.77	T_{2m} (3Si,1Al)
−100.9	28.01	T_{1m} (3Si,1Al)
−101.9	5.97	T_{10} (3Si,1Al)

[a] Chemical shift (peak position) are in parts per million (ppm) from tetramethylsilane (TMS) as external standard spectrum of sample. Integrated intensities are in relative values. Structural sites are as crystallographic nonequivalent positions with their chemical environments.

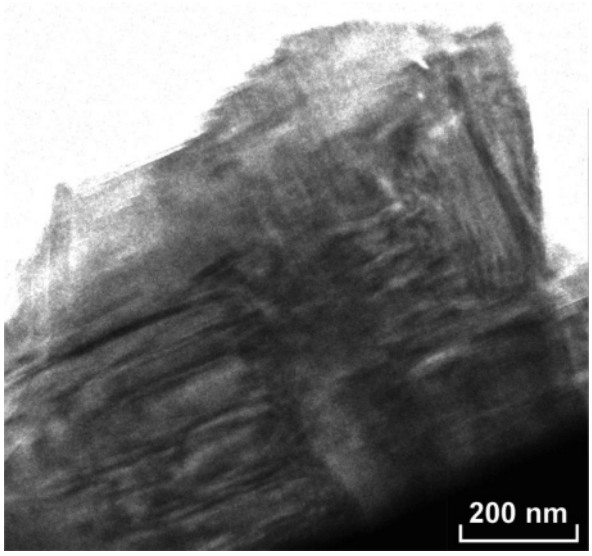

Figure 2. Bright field low-resolution image along the [001] zone displaying a heterogeneous and irregular microstructure due to an orthogonal modulated structure with wavelike contrast, which defines Albite and Pericline twin-domains in the intermediate microcline LS176. This image corresponds to the SAED pattern of Figure 3.

Figure 3 exhibits the SAED pattern taken along the [001] direction showing modulations along (hk0) planes, with diffuse streaks parallel to the a^* and b^* axes, which correspond to discrete crystalline domains of microcline following the Albite and Pericline twin laws (M-twinning). The sharp resolution of two peaks was produced in reflections far away from the origin. The γ^* angle (triclinicity) was also measured in these patterns. We observe the γ^* angle deviates clearly from monoclinic symmetry, giving a value of ∼91° characteristic of the intermediate microcline variety. The presence of a diffuse streak along the two mentioned directions is presumably due to the disordered, strained, and defect-rich material located between domains.

Luminescence Spectra Techniques. A comparison between natural TL (NTL) and X-ray induced TL (ITL) spectra of the triclinic K-feldspar was made using 3D-TL plots

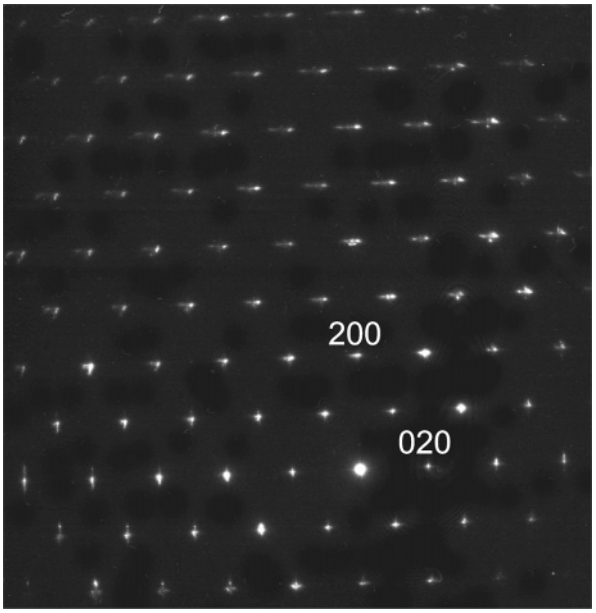

Figure 3. Selected area electron diffraction (SAED) pattern along the [001] zone for the microstructure (Figure 6) of sample LS176 with X-ray pattern of triclinic intermediate microcline $\Delta = 0.78$.

displaying intensity I (in au) versus temperature T (in °C) versus wavelength λ (in nm) in Figure 4a and c and contour plots in the wavelength−temperature section in Figure 4b and d. The observed emissions in NTL are negligible with the exception of some UV spectral bands, mainly at higher temperatures over 200 °C (Figure 4a and b). The ITL spectrum recorded after 50 Gy X-ray irradiation shows four different emissions: (i) a sharp signal at ∼290 nm, with the maximum intensity at around 110 °C, and several low intensity peaks at about 340 nm detected in the UV region; (ii) a weak broad blue band was observed at 120 °C; (iii) the weak green emission appears at ∼570 nm showing complex multi-order kinetics with maxima at 110 and ∼300 °C; and (iv) a very weak signal at around 630 nm.

The RL and CL spectra (Figure 5) are formed by two maxima at ∼290 and 570 nm and a small shoulder at ca. 630 nm. The relative intensity of the UV and green bands changes with the type of luminescence experiment. The main differences between "delayed" (TLI and TLN) and "prompt" (RL and CL) spectra lie in the main peaks observed in the curves. Thus, the most important contribution in TL emission corresponds to the well-defined UV emission; meanwhile, the green emission appears as the more intense peak in the RL and CL processes. An important characteristic of this sample is the very weak emission of the blue broad band, which is characteristic in K-rich feldspars.

Figure 6a shows the asymmetric shape of the ITL glow peak at 290 nm after 50 Gy X-ray irradiation (Figure 4c) in which two contrasting parts can be distinguished at both sides of the maxima, that is, exponential versus logarithmic. At lower temperatures (from room temperature to 110 °C), the initial rise method (IRM) showed an Arrhenius behavior: $\ln I = \ln s - E_a/kT$ (where s is the pre-exponential factor, and E_a is the thermal activation energy). The activation energy E_{act} obtained between 70 and 106 °C was 1.14 ± 0.03 eV (Figure 3b). In the high-temperature side, the power law method (PLM) showed the dependence $\log I = -\tau \log T$ plot (where τ is the coefficient). In this analysis, a value of $\tau \approx 6$ was obtained, indicating a complex kinetic process. The observed behavior has frequently been observed in other K-feldspars but not in Na-feldspar.

Discussion

The interpretation of the 290 nm emission band of microclines in previously published articles must be revised because most of them use heterogeneous perthites as working samples. Perthites are composed by a major matrix phase, that is, the K-rich feldspar, and a minor exsolved phase, that is, the Na-rich feldspar, as discrete regions. Note that the 290 nm band is also a typical emission of triclinic Na-feldspar crystals. In addition, an explanation that takes into account structural characteristics has to be considered, because the intensity of the signal shows a clear correlation with the structural state of the K-feldspars: the 290 nm band is absent in monoclinic sanidine, it has low intensity in high microcline with modulated structure, and it has a higher intensity in triclinic twinned low microcline.[16,18,19]

Here, we have selected a homogeneous K-feldspar without Na-feldspar impurities, which have suffered the monoclinic−triclinic transformation (MTT), to clarify the appearance of the luminescence signal in K-feldspars. The possible relationship of the UV emission band with Pb or Tl point defects was avoided in our sample from the low concentration of these ions detected in the chemical analyses. Therefore, the appearance of this UV luminescence must be related "at least" to the transformation of sanidine into low microcline, in which two separated steps can be considered, as follows: first, a diffusive step (Si/Al ordering) produces the inversion of sanidine into high microcline ca. 450 °C by a cooperative structural collapse. This first material produced with triclinic symmetry and disordered Si/Al distribution is formed by a heterogeneous perturbed lattice without discrete wall boundaries that evolve to a nanodomain structure with ill-defined wall boundaries,[11] that is, the so-called "tweed" microstructure. In these "metastable" K-feldspars, the 290 nm band could be absent or very weak.[25] A second step occurs by severe recrystallization where high microcline is transformed into low microcline in a discontinuous way, accompanied by intense Si/Al ordering.[9] Furthermore, following Ostwald's law, between high and low microcline, frequently unstable transitional intermediate microclines occur.[26] The "stable" phase at low temperature, that is, low microcline, shows the highest intensity in the 290 nm band. These ordered microclines exhibit twin-domains defined by the Albite and Pericline twin laws. The Albite twin law is a rotation of 180° about b^*, and the Pericline law is a rotation of 180° about b. Thus, the (010) twin (compositional) plane of the Albite twins is perpendicular to the [010] twin axis of the Pericline twins in inversion domain structures. Pericline twins are in contact by the rhombic section, a boundary parallel to the twin axis, with irrational orientation.[9] The atoms in the twin boundaries may be less strongly held in place than those in the bulk lattice.[27]

(25) Correcher, V.; García-Guinea, J. *J. Lumin.* **2001**, *93*, 303−312.
(26) Senderov, E. E. *Bull. Soc. Fr. Mineral. Cristallogr.* **1974**, *97*, 393−402.

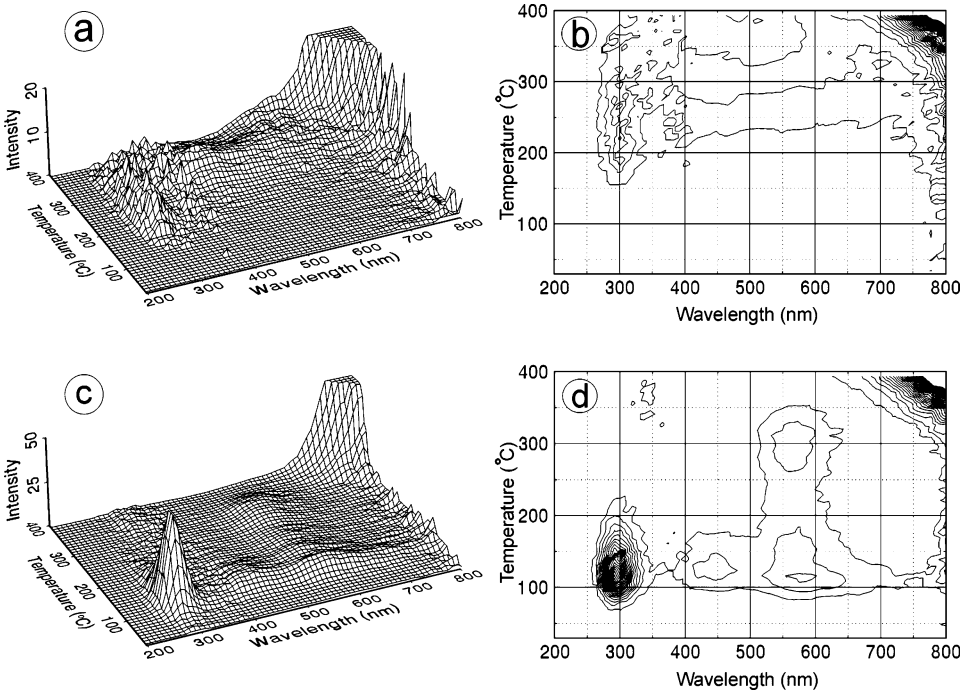

Figure 4. TL spectra of LS176 (intermediate microcline): (a) isometric plot of the natural TL; (b) contour plot of the natural TL; (c) isometric plot after 50 Gy X-ray dose; and (d) contour plot after 50 Gy X-ray dose. These data were recorded at a heating rate of 2.5 °C s^{-1}.

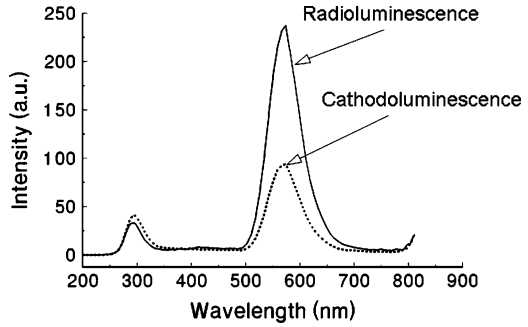

Figure 5. RL and CL spectra of the sample LS176 (intermediate microcline) recorded between 200 and 800 nm, with wavelength in nanometers and intensity in arbitrary unit (au).

In this work, a transitional product of the Si/Al ordering process, that is, intermediate microcline, displays the 290 nm luminescence emission band. This material has a local T−O−T geometry very similar to disordered microclines,[11,28] as the chemical shifts of the ^{29}Si spectrum indicate (Figure 1). Specific Si/Al local configurations from the ordering processes cannot explain the appearance of this emission band because perfectly ordered low microclines from authigenic origin do not show any luminescence, that is, crystallized without a monoclinic precursor and then lacking of twin-domain microstructures. Therefore, because local structural changes and Si/Al ordering cannot explain the appearance and intensity increase of the 290 nm emission band while the MTT progress, it is reasonable to associate the UV band with the formation of the wall boundaries among twin-domains. Optically active inversion domain boundaries have been already described in other organic and inorganic materials.[29,30] In this work, we propose that the increase in intensity of the 290 nm band is related to the redistribution of the structural strain during the K-feldspars recrystallization: initially wide and irregular boundaries with small and dispersed structural strain evolve to a full accommodation of strain in the twin-domain boundary with sharp and regular walls.

This structural adjustment with regions of high free-energy should provide "stability" to some defects acting as active centers, at the compositional plane of the twinned domains. Albite twins are in contact by walls parallel to (010) planes that can show anomalously high Na contents.[23] These Na-rich boundaries could be also the site of other defects including chemical impurities and oxygen O^{2-} vacancies, and hole centers related to oxygen defect sites, in which a trapped electron could produce emissions at 290 nm, which is also typical in silica.[31] Data from luminescence experiments could give some information about the nature of such centers. "Delayed" processes are more sensible to their activation than "prompt" processes. The ITL spectrum shows that the different bands peak at distinct temperatures, forming temperature−wavelength pairs. Assuming that the radiative recombination is associated with oxygen vacancies, the calculated activation energy of 1.14 eV could be related to the Na motion[16] and not with oxygen diffusion as in the silica case.[32] In addition, feldspars display an intense optical absorption in this region of the UV, which results from electrons trapped probably at O^{2-} vacancies and from hole centers linked to several oxygen defect sites.[33] Finally,

(27) Lee, W. T.; Salje, E. K. H.; Bismayer, U. *J. Phys.: Condens. Matter* **2003**, *15*, 1353−1366.
(28) Xiao, Y.; Kirkpatrick, R. J.; Hay, R. L.; Joong Kim, Y. *Mineral. Mag.* **1995**, *59*, 47−61.
(29) Breu, J.; Stossel, P.; Schrader, S.; Starukhin, A.; Finkenzeller, W. J.; Yersin, H. *Chem. Mater.* **2005**, *17*, 1745−1752.
(30) Schuck, P. J.; Mason, M. D.; Grober, R. D.; Ambacher, O.; Lima, A. P.; Miskys, C.; Dimitrov, R.; Stutzmann, M. *Appl. Phys. Lett.* **2001**, *79*, 952−954.
(31) Jones, C. E.; Embree, D. *J. Appl. Phys.* **1976**, *47*, 5365−5371.
(32) Griscom, D. L. *Phys. Rev. B* **2001**, *64*, art. 174201.
(33) Hofmeister, A. M.; Rossman, G. R. *Am. Mineral.* **1986**, *71*, 95−98.

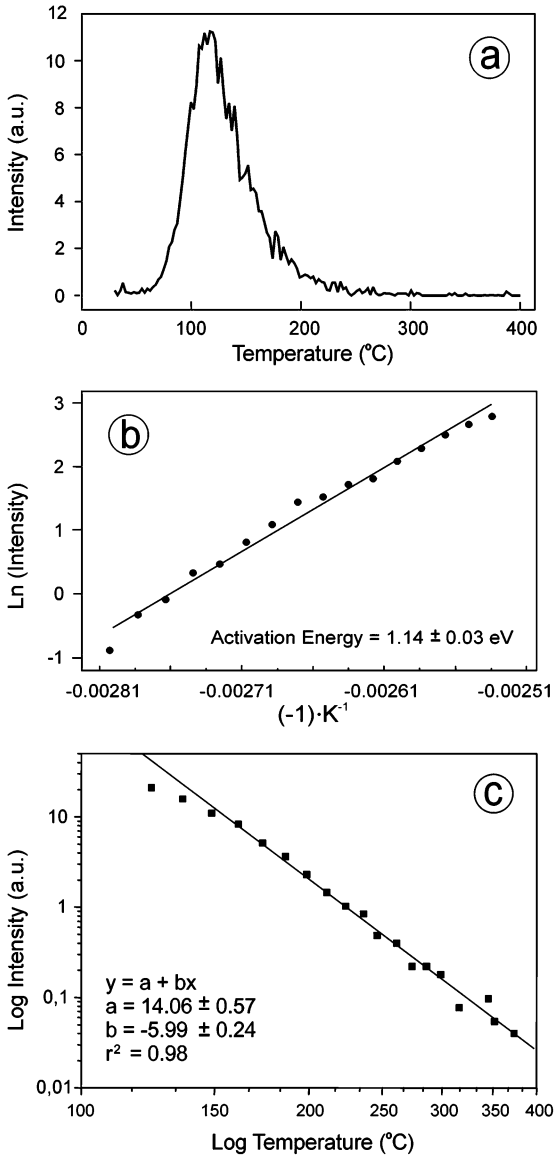

Figure 6. (a) TL slice at 290 nm obtained from the ITL spectrum of Figure 4c between room temperature and 400 °C showing a clear asymmetric shape in the glow curve. (b) Low-T side of the TL curve of (a) with an exponential analysis using the initial rise method (IRM) and an Arrhenius plot of ln $I = \ln s - E_a/kT$ (where s is the pre-exponential factor, and E_a is the thermal activation energy) with $E_a = 1.14 \pm 0.03$ eV. (c) High-T side of the TL slice of curve in (a) with a double logarithmic analysis in intensity I and temperature T by a power law method (PLM) using a log $I = -\tau \log T$ plot (where τ is the coefficient), with the parameters of the corresponding lineal fitting $y = a + bx$ as follows: $a = 14.06 \pm 0.57$; $b = -5.99 \pm 0.24$ (parameter τ), and $r^2 = 0.98$.

electron−hole pairs at these interfaces have to be associated with local structural distortion in the lattice to accommodate the weakening of bonds (strain). The locally strained lattice around coherent wall boundaries could be stabilized by association with other local structural entities. These observations suggest a strong correlation between different defects, that is, structural complexes of defects formed at wall boundaries between twin-domains.

These active structural complexes could explain the thermal decay following a power law statistics as a distinctive character in comparison with point defects luminescence, in which first- and second-order kinetics are considered. Electron avalanches associated with a cooperative behavior inside the complexes with scaling probability distributions for their detrapping decay are compatible with wall dynamics, as observed in other domain structures. This explanation is also compatible with the fractal regime of other systems in which the recombination process is diffusion-limited,[34] as occurs in this case by Na ions.

Conclusions

The origin of the ultraviolet UV light emission luminescence at 290 nm in a K-feldspar (adularia type) with chemical formula $K_{0.98}Na_{0.02}Al_{1.02}Si_{2.98}O_8$ obtained from the EMPA technique is here explored. The characterization techniques (XRD, TEM, SAED patterns, and ^{29}Si MAS NMR) indicate that this material is an intermediate microcline with irregular submicroscopical twinning and a triclinic local unit cell. The spectroscopic techniques (TL, RL, and CL) display the appearance of intense emission bands peaked at 290 and 570 nm. The more relevant findings related to the UV band are: (i) A close association between twinning and the UV luminescence has been established, pointing to charge trapping and light emissions from complexes of structural defects located in the twin-domain boundaries. (ii) The induced TL spectrum recorded after 50 Gy X-ray irradiation exhibits an asymmetric glow curve, with two contrasting parts at both sides of the maximum. The low-temperature part follows an exponential rise, and the high-temperature slope follows a power law decay. (iii) A possible trapping−detrapping dynamic process related to cooperative phenomena inside the complexes has been proposed to explain such decay, in which the recombination process is Na ion diffusion-limited.

Acknowledgment. We are grateful to Prof. Dr. P. D. Townsend for the analyses in the high sensitivity thermoluminescence spectrometer of Sussex (UK) and M. L. Clarke for recording the 3D-TL measurements. The experimental work was supported by the C.I.C.Y.T. CGL2004-03564/BTE project. Thanks are also due to Martin Fernandez (Colmenar Viejo, Madrid) for valuable help in the collection of samples.

CM060246O

(34) Griscom, D. L.; Gingerich, M. E.; Friebele, E. J. *Phys. Rev. Lett.* **1993**, *71*, 1019−1022.